Mucosally transplanted mesenchymal stem cells stimulate intestinal healing by promoting angiogenesis

Nicholas A. Manieri,[1] Madison R. Mack,[1] Molly D. Himmelrich,[1] Daniel L. Worthley,[2,3] Elaine M. Hanson,[4] Lars Eckmann,[4] Timothy C. Wang,[2] and Thaddeus S. Stappenbeck[1]

[1]Department of Pathology and Immunology, Washington University School of Medicine, St. Louis, Missouri, USA. [2]Department of Medicine, Columbia University Medical Center, New York, New York, USA. [3]Department of Medicine, University of Adelaide, South Australia, Australia. [4]Department of Medicine, UCSD, La Jolla, California, USA.

Mesenchymal stem cell (MSC) therapy is an emerging field of regenerative medicine; however, it is often unclear how these cells mediate repair. Here, we investigated the use of MSCs in the treatment of intestinal disease and modeled abnormal repair by creating focal wounds in the colonic mucosa of prostaglandin-deficient mice. These wounds developed into ulcers that infiltrated the outer intestinal wall. We determined that penetrating ulcer formation in this model resulted from increased hypoxia and smooth muscle wall necrosis. Prostaglandin I_2 (PGI_2) stimulated VEGF-dependent angiogenesis to prevent penetrating ulcers. Treatment of mucosally injured WT mice with a VEGFR inhibitor resulted in the development of penetrating ulcers, further demonstrating that VEGF is critical for mucosal repair. We next used this model to address the role of transplanted colonic MSCs (cMSCs) in intestinal repair. Compared with intravenously injected cMSCs, mucosally injected cMSCs more effectively prevented the development of penetrating ulcers, as they were more efficiently recruited to colonic wounds. Importantly, mucosally injected cMSCs stimulated angiogenesis in a VEGF-dependent manner. Together, our results reveal that penetrating ulcer formation results from a reduction of local angiogenesis and targeted injection of MSCs can optimize transplantation therapy. Moreover, local MSC injection has potential for treating diseases with features of abnormal angiogenesis and repair.

Introduction

Mesenchymal stem cells (MSCs) are an enticing potential therapeutic agent for a variety of inflammatory conditions, including those that occur in the gastrointestinal tract. MSCs are currently being tested as a cellular therapy in chronic intestinal diseases, such as complicated fistulas and inflammatory bowel disease (1, 2). Key clinical questions involving MSC transplantation include the ideal route of delivery, tissue source, cell number, and the frequency of injection. What has stymied progress is the lack of understanding of the specific factors produced by MSCs that functionally affect intestinal repair. A more complete understanding of the basic mechanisms of intestinal repair in normal and pathological settings will allow for better targeted use of MSC therapies.

MSCs were initially transplanted into patients with inflammatory/degenerative diseases because of their unique stem cell characteristics, as determined by in vitro studies. MSCs are fibroblast-like cells that are capable of self-renewal and differentiation into several mesenchymal lineages (3). They are capable of migrating to sites of inflammation and injury and are thought to be nonimmunogenic because they can be transplanted through intravenous or local injection into allogeneic hosts (4). Despite promising outcomes in animal and early clinical trials, the majority of intravenously injected MSCs became trapped in the lung, limiting their ability as tissue stem cells (5, 6).

Now, the main mechanism of how transplanted MSCs function is considered to be secretion of proregenerative and antiinflammatory factors (3, 4, 6, 7). While MSCs secrete several anti-inflammatory factors that can act at a long distance (e.g., IL-10 and antiinflammatory protein TSG-6), they also produce several factors that are short-lived in the bloodstream (e.g., VEGF-A and prostaglandins) (4). Depending on the disease and organ affected, MSCs may need to migrate directly to an area of injury and secrete factors locally to reach maximal therapeutic outcomes.

To study the role of transplanted MSCs in stimulating intestinal repair, we used an acute injury model that focally injures the colonic mucosa through endoscopy-directed biopsy. To initiate injury, forceps physically remove a small fragment of the distal colon mucosa, while leaving the underlying muscularis propria intact. A major strength of this experimental system is that it is amenable to quantitative analysis of in vivo lesions due to the precise timing and location of mucosal damage and repair (8–13). Thus, the in vivo mechanisms of mucosal repair are tractable using this model. We previously found that focal injury induced by biopsy (biopsy injury) in prostaglandin-deficient mice leads to penetrating ulcers that develop around 6 days after the initial injury (14). As we ultimately wanted to use MSC transplantation to stimulate repair in this model, we first needed to determine the mechanism of penetrating ulcer formation.

Penetrating ulcers can occur throughout the gastrointestinal tract and are associated with chronic inflammation (15, 16) and inhibition of prostaglandin production (17, 18), though the mechanisms for how they form are unknown. The two rate-limiting enzymes for prostaglandin production, prostaglandin-endoperoxide synthase 1

Conflict of interest: The authors have declared that no conflict of interest exists.
Submitted: February 13, 2015; **Accepted:** July 8, 2015.
Reference information: *J Clin Invest*. 2015;125(9):3606–3618. doi:10.1172/JCI81423.

and 2 (PTGS1 and PTGS2, also known as COX-1 and COX-2), are inhibited by NSAIDs (19). NSAIDs and PTGS2-specific inhibitors are associated with gastrointestinal ulcers that can penetrate the outer smooth muscle wall (muscularis propria) (20, 21). Such penetrating ulcers result in replacement of the muscle wall with immature blood vessels and macrophages, termed granulation tissue (15, 22). NSAIDs are typically associated with gastric and duodenal ulcers, but the use of slow-release NSAIDs can result in lesions in the distal small intestine and colon, suggesting that there may be a common mechanism of NSAID-induced ulceration in the gastrointestinal tract (21). Understanding how penetrating ulcers form may help prevent their formation and improve therapies designed to accelerate ulcer healing, such as MSC transplantation.

Here, we first took an in vivo approach to determine the mechanism of penetrating ulcer formation. We found that prostaglandin I_2 (PGI_2) was necessary to prevent penetrating ulcers after colonic biopsy injury. We found that, within injured *Ptgs2*$^{-/-}$ and PGI_2 receptor knockout (*Ptgir*$^{-/-}$) mice, defective VEGF-dependent angiogenesis led to local tissue hypoxia and smooth muscle necrosis. We used knowledge of this mechanism to design additional experiments to test the role of transplanted MSCs in mucosal repair. We found that, in contrast to intravenously injected colonic MSCs (cMSCs), mucosally transplanted cells robustly migrated to wounds and rescued penetrating ulcer formation. This rescue was dependent on VEGF expression in the transplanted cMSCs. These results show that proper angiogenesis is required for intestinal repair after injury and that mucosally transplanted MSCs can migrate to sites of injury in the intestine to stimulate VEGF-dependent angiogenesis and proper regeneration.

Results

PGI_2 is required to prevent penetrating ulcers after colonic mucosal injury. We previously showed that colonic mucosal injury of *Ptgs2*$^{-/-}$ mice led to penetrating ulcers, as highlighted by loss of α–smooth muscle actin (α-SMA [*Acta2*]) staining within the underlying muscularis propria (Figure 1, A and B). This was not an immediate consequence of injury, as α-SMA loss occurred 6 days after biopsy injury (14). In our previous study, coadministration of two stable prostaglandin analogs of PGE_2 and PGI_2 prevented loss of staining in the muscularis propria of mucosally injured *Ptgs2*$^{-/-}$ mice (14).

Here, we determined that PGI_2 was the critical prostaglandin for smooth muscle protection after mucosal injury. Vehicle-injected mice showed expected phenotypes at day 6 after injury; WT controls showed minimal damage (Figure 1C), while *Ptgs2*$^{-/-}$ mice showed extensive damage, as quantified by loss of α-SMA staining in the outer longitudinal layer of the muscularis propria (Figure 1D). In experimental groups, the α-SMA staining underlying wounds from *Ptgs2*$^{-/-}$ mice injected with stable analogs of PGI_2 was similar to that of WT mice, while wounds from *Ptgs2*$^{-/-}$ mice injected with multiple doses of stable analogs of PGE_2 were similar to those of vehicle-injected *Ptgs2*$^{-/-}$ mice (Figure 1, E–G, and Supplemental Figure 1). These results showed that PGI_2 analogs prevented damage to the muscle wall of biopsy-injured *Ptgs2*$^{-/-}$ mice (Supplemental Figure 2).

We next injured *Ptgir*$^{-/-}$ mice (23) that lack the single receptor for PGI_2. Colonic mucosal injuries of *Ptgir*$^{-/-}$ mice showed extensive loss of α-SMA staining at day 6 after injury, while littermate *Ptgir*$^{+/+}$ mice showed minimal evidence of muscle wall damage (Figure 1, H and I). These results show that PGI_2 was required to prevent loss of α-SMA staining in the muscularis propria after colonic biopsy injury.

Loss of α-SMA is due to colonic smooth muscle necrosis. We next confirmed that the loss of α-SMA staining in *Ptgs2*$^{-/-}$ colonic injuries was due to smooth muscle cell death. To perform smooth muscle cell–tracing experiments, we generated *Acta2-CreER*^{T} knockin mice and bred them to *R26*$^{mT/mG}$ reporter mice (24). After tamoxifen induction, virtually all α-SMA–positive cells of uninjured colons were EGFP positive (Supplemental Figure 3A), a finding observed throughout the gastrointestinal tract (Supplemental Figure 3, B–G). We injured tamoxifen-induced *Acta2-CreER*^{T} *R26*$^{mT/mG}$ mice and treated them with either the selective PTGS2 inhibitor NS-398 (25) (that led to comparable healing defects as in injured *Ptgs2*$^{-/-}$ mice; Supplemental Figure 4) or vehicle. At day 6 after injury, we evaluated the localization of EGFP and α-SMA expression in the muscularis propria. In vehicle-treated controls, smooth muscle cells beneath the wound bed coexpressed EGFP and α-SMA (Figure 2, A and B). In NS-398–treated mice, α-SMA staining was focally lost within the muscularis propria immediately beneath the wound as expected (Figure 2, C and D). In this same area, EGFP staining was no longer detected in all the wounds examined, indicating that the smooth muscle cells had died and not downregulated α-SMA by dedifferentiation.

The smooth muscle cell death in mucosa-injured *Ptgs2*$^{-/-}$ mice occurred primarily by necrosis. We evaluated H&E-stained sections of WT and *Ptgs2*$^{-/-}$ mice to examine histologic hallmarks of necrosis, which preceded the eventual loss of smooth muscle cells, at 2 and 4 days after injury. No signs of smooth muscle necrosis were detected in any of the wound sections from WT or *Ptgs2*$^{-/-}$ mice 2 days after injury (Supplemental Figure 5). Four days after injury, injured WT mice showed little evidence of coagulative necrosis (Figure 2, E and F), whereas *Ptgs2*$^{-/-}$ wounds showed areas of coagulative necrosis in the area of the original muscularis propria (Figure 2, G–I). The key histologic features were replacement of smooth muscle cells with eosinophilic material that lacked the typical elongated nuclei of smooth muscle cells. In addition, at day 4 after injury, WT and *Ptgir*$^{-/-}$ mice showed no difference in smooth muscle cell proliferation, further supporting a primary role for cell death in this phenotype (Supplemental Figure 6). We also considered the possibility that smooth muscle cells in *Ptgs2*$^{-/-}$ mice died via other mechanisms. At day 2 after injury, wounds from *Ptgs2*$^{-/-}$ mice contained more cleaved caspase-3–positive cells in the muscularis propria (Supplemental Figure 7). However, by day 4 after injury (when the muscularis propria was still intact), wounds of WT and *Ptgs2*$^{-/-}$ mice contained similar numbers of cleaved caspase-3–positive cells in the muscularis propria. In addition, there was no evidence of increased necroptosis in PTGS2-inhibited biopsy-injured mice (Supplemental Figure 8). Because of the temporal relationship between necrosis and muscle loss in *Ptgs2*$^{-/-}$ mice, we focused on mechanisms related to necrosis.

Defective angiogenesis in mucosal wounds results in hypoxia and penetrating ulcers. Coagulative necrosis most commonly occurs in tissues secondary to localized ischemia. We stained wounds from

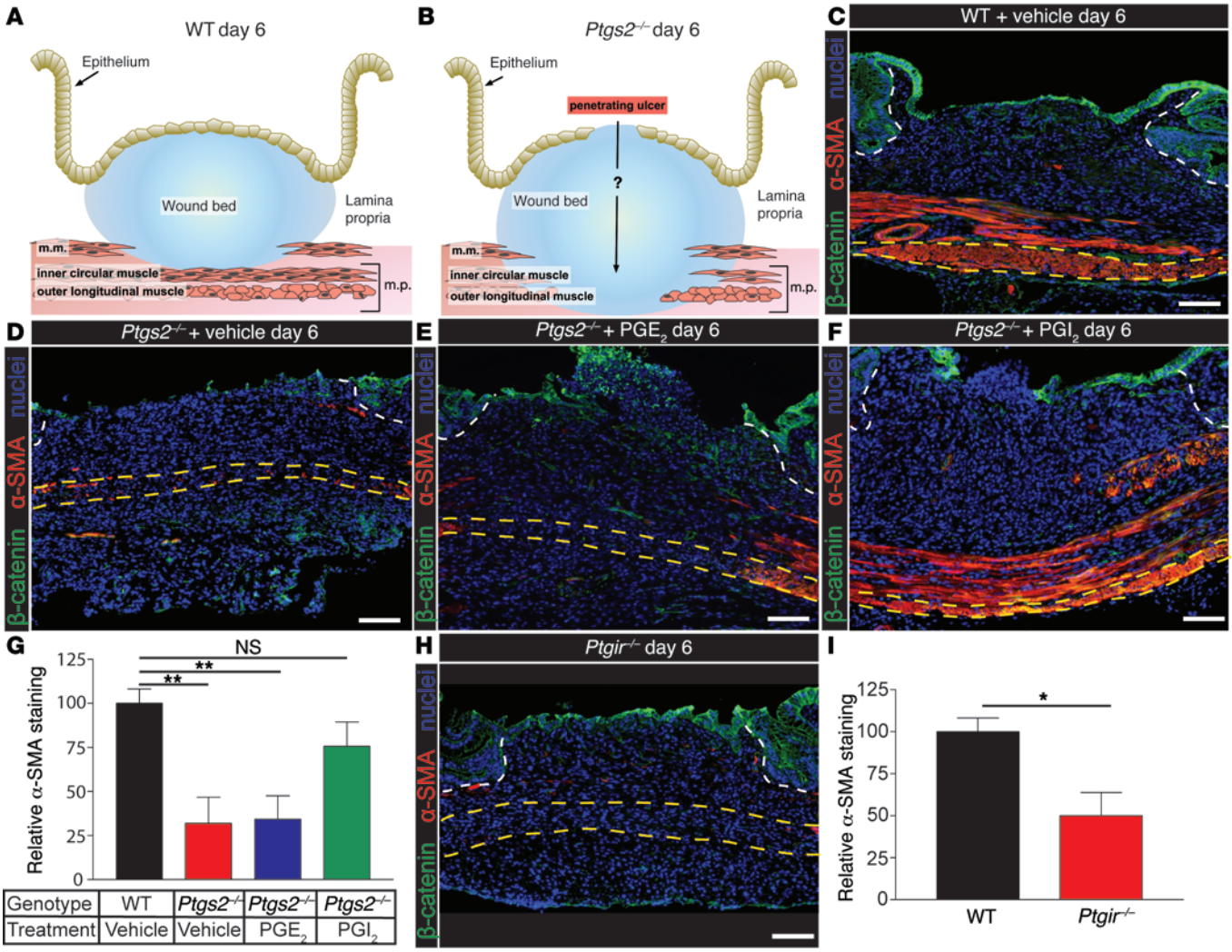

Figure 1. PGI_2 is necessary to prevent loss of α-SMA staining after mucosal injury. Wounds 6 days after injury in (**A**) WT and (**B**) *Ptgs2*$^{-/-}$ mice. Muscularis propria loses α-SMA staining beneath wounds in *Ptgs2*$^{-/-}$ mice within 6 days. Mechanisms leading to penetrating ulcer formation in this model are not known. m.m., muscularis mucosae (removed during biopsy); m.p., muscularis propria (containing an inner circular and outer longitudinal layer, not removed during biopsy). (**C**–**F**) Representative images of colonic sections (n = 9 wounds per group in 4 experiments) 6 days after injury from (**C**) WT (n = 5 mice) or (**D**–**F**) *Ptgs2*$^{-/-}$ mice treated with (**C** and **D**) vehicle (n = 6 mice), (**E**) 100 μg/kg PGE_2 analog (n = 4 mice), or (**F**) 200 μg/kg PGI_2 analog (n = 4 mice). Sections were stained with anti–β-catenin antisera (green, epithelium), anti–α-SMA antisera (red, smooth muscle cells), and bisbenzimide (blue, nuclei). Dashed white lines outline wound beds. Dashed yellow lines outline outer muscle (quantified in **G**). (**G**) Relative α-SMA staining in outer muscle layer underlying wounds from indicated groups of mice. n = 9 wounds per group from 4 to 6 mice per group in 4 experiments; mean ± SEM. P = 0.0039 by 1-way ANOVA. $^{**}P < 0.01$, Tukey's post-test. (**H**) Representative image of *Ptgir*$^{-/-}$ colon (n = 10 wounds from 6 mice in 3 experiments) 6 days after biopsy stained with anti–β-catenin antisera (green), anti–α-SMA antisera (red), and bisbenzimide (blue). (**I**) Relative α-SMA staining of the outer muscle layer in WT and *Ptgir*$^{-/-}$ mice 6 days after injury. Mean ± SEM. $^{*}P < 0.05$, Student's t test. WT samples: n = 6 wounds from 4 mice in 3 experiments; *Ptgir*$^{-/-}$ samples: n = 10 wounds from 6 mice in 3 experiments. Scale bar: 100 μm.

WT, *Ptgs2*$^{-/-}$, and *Ptgir*$^{-/-}$ mice 4 days after injury with HIF-1α antisera to detect hypoxic cells (26). The surface epithelium of the mouse colon is hypoxic, likely due to the anaerobic nature of the lumen (27). All mice in all groups showed readily detectable HIF-1α staining in surface epithelial cells, covering both wounded and nonwounded areas (Figure 3, A–F). At day 4 after injury, *Ptgs2*$^{-/-}$ and *Ptgir*$^{-/-}$ mice showed abundant HIF-1α–positive cells that were concentrated in the area of the muscularis propria and an underlying area of expanded serosa (Figure 3, C–F). In contrast, similarly injured WT mice showed far fewer HIF-1α–positive cells in this area of the wound (Figure 3G). As additional evidence for hypoxia at this time point, 2 hours before sacrifice, we injected groups of *Ptgs2*$^{-/-}$ and WT mice with a nitroimidazole that detects hypoxic cells [2-(2-nitro-1H-imidazol-1yl)-N-(2,2,3,3,3-pentafluoropropyl) acetamide (EF5)] (28). EF5 is retained within hypoxic cells by nonspecific binding to intracellular macromolecules, and this compound can be detected by immunofluorescence localization with an anti-EF5 antibody (28). We found that wounds from *Ptgs2*$^{-/-}$ mice had significantly more EF5-positive cells than WT mice at day 4 after injury (Supplemental Figure 9). These two independent assays showed that the colonic wound beds of *Ptgs2*$^{-/-}$ mice were hypoxic.

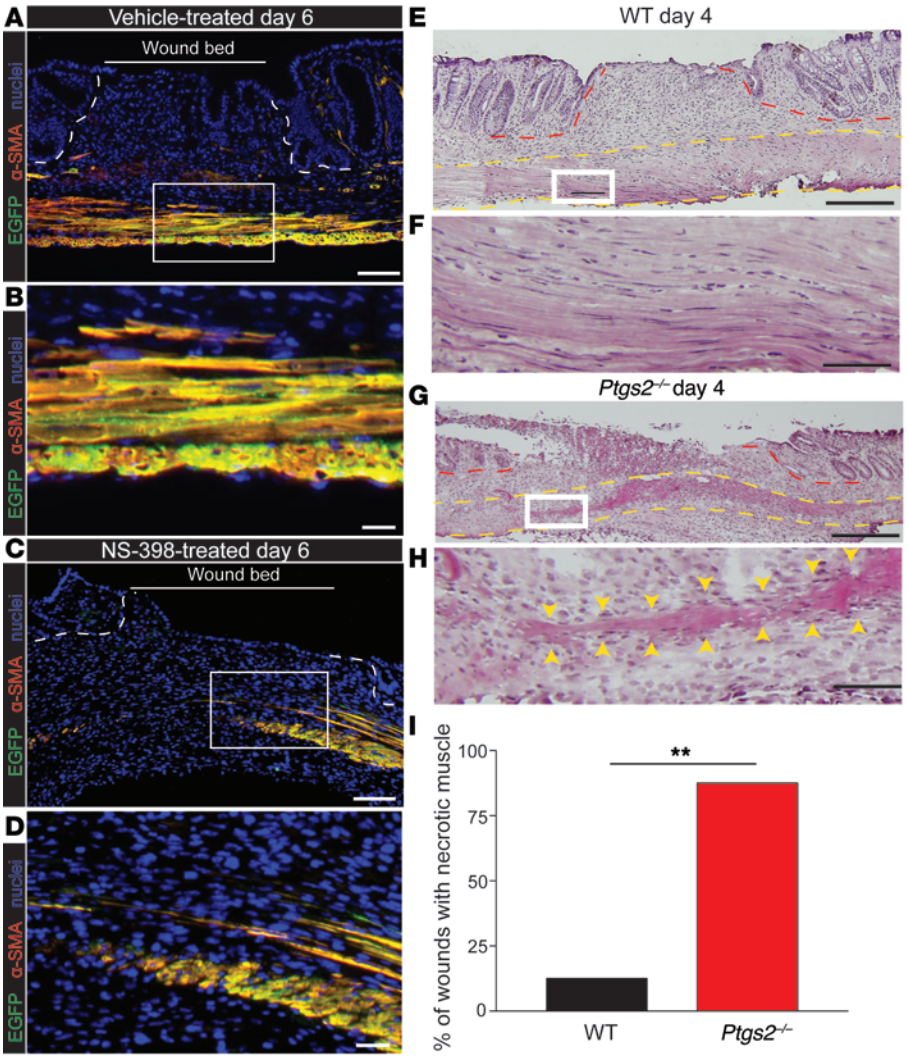

Figure 2. Colonic smooth muscle cells die via necrosis in mucosally injured *Ptgs2*$^{-/-}$ mice. (**A**–**D**) Representative images of colonic sections from *Acta2-CreER*^{T} *R26*$^{mT/mG}$ mice that were injected with (**A**) vehicle or (**C**) the PTGS2 inhibitor, NS-398, for 6 days after biopsy injury. *Acta2-CreER*^{T} *R26*$^{mT/mG}$ mice were injected with tamoxifen 2 weeks prior to colonic biopsy injury to permanently label α-SMA–expressing smooth muscle cells (green), and sections from PTGS2-inhibited or vehicle-treated mice 6 days after injury were stained with anti–α-SMA antisera (red, smooth muscle cells) and bisbenzimide (blue, nuclei). Dashed white lines outline the edges of the wound bed, and the solid white box indicates the areas shown at higher magnification in **B** and **D**. *n* = 6 wounds per group from 3 mice per group in 3 experiments. (**E**–**H**) Representative H&E-stained images of colonic sections from (**E**) WT or (**G**) *Ptgs2*$^{-/-}$ mice 4 days after injury. The wound bed is outlined in dashed red lines, the muscularis propria is outline in dashed yellow lines, and the areas shown at higher magnification in **F** and **H** are labeled by solid white boxes. The yellow arrowheads in **H** indicate areas of necrotic tissue. *n* = 8 wounds per group from 3 mice per group in 3 experiments. (**I**) Percentage of wounds that contained areas of necrosis at day 4 by H&E staining. *n* = 8 wounds per group from 3 mice per group in 3 experiments. $^{**}P < 0.01$ by χ^2 test for presence or absence of necrosis. Scale bar: 100 μm (**A** and **C**); 25 μm (**B**, **D**, **F**, and **H**); 200 μm (**E** and **G**).

We hypothesized that hypoxia in *Ptgs2*$^{-/-}$ and *Ptgir*$^{-/-}$ colonic wounds resulted from defective angiogenesis. We found that WT mice contained abundant CD31-positive endothelial cells located in the central wound bed 4 days after biopsy (Figure 3H). However, *Ptgs2*$^{-/-}$ and *Ptgir*$^{-/-}$ mice had significantly fewer CD31-positive cells in their central wound beds at this time point (Figure 3, I–K). These data suggested that local hypoxia in *Ptgs2*$^{-/-}$ and *Ptgir*$^{-/-}$ wounds was due to defective angiogenesis. We next stained wounds for VEGF, a critical factor for angiogenesis (29). We detected fewer VEGF-expressing cells in the wound beds of *Ptgs2*$^{-/-}$ and *Ptgir*$^{-/-}$ mice at day 4 after injury as compared with those in WT controls (Figure 3L and Supplemental Figure 10). As many cell types can express VEGF, including macrophages (22) and fibroblasts (30), we additionally stained WT wounds for F4/80 to label macrophages. We found that VEGF-expressing cells included F4/80-positive macrophages and F4/80-negative cells with fibroblast morphology (Supplemental Figure 11), indicating that there were multiple VEGF-expressing cell types within wounds. These data showed that PGI_2 signaling was necessary to stimulate VEGF expression within mucosal wounds during repair.

To functionally show that hypoxic damage caused muscle necrosis, we inhibited angiogenesis in WT mice with tivozanib, a pan-VEGFR tyrosine kinase inhibitor (31). Vehicle-treated mice 4 days after injury showed abundant blood vessels within wound beds and scant HIF-1α–positive cells within the muscularis propria as expected (Figure 4, A and B). In contrast, VEGFR inhibitor–treated mice showed fewer blood vessels within the center of mucosal wounds and more abundant HIF-1α–positive cells (Figure 4, C–F). Importantly, at day 6 after injury, smooth muscle necrosis occurred in VEGFR inhibitor–treated mice as compared with that in vehicle-treated controls (Figure 4, G and H). At day 6 after injury, we found that PGI_2 analogs could not rescue the smooth muscle necrosis in VEGFR-inhibited mice (Figure 4, I and J). This result suggested that PGI_2 did not act directly on the smooth muscle cells to prevent smooth muscle necrosis and that PGI_2 was upstream of VEGF-induced angiogenesis. Since modulating epithelial proliferation can also impact colonic wound repair (11–13, 32), we measured the percentage of Ki67-positive epithelial cells immediately adjacent to WT and *Ptgir*$^{-/-}$ day 4 wounds and found no significant differences (Supplemental Figure 12). Taken together, these results showed that defective angiogenesis in mucosal wounds led to local hypoxia and subsequent smooth muscle necrosis (Figure 4K).

Mucosally injected cMSCs migrate to wound beds and prevent penetrating ulcers in Ptgir$^{-/-}$ *mice*. Knowing the key elements of

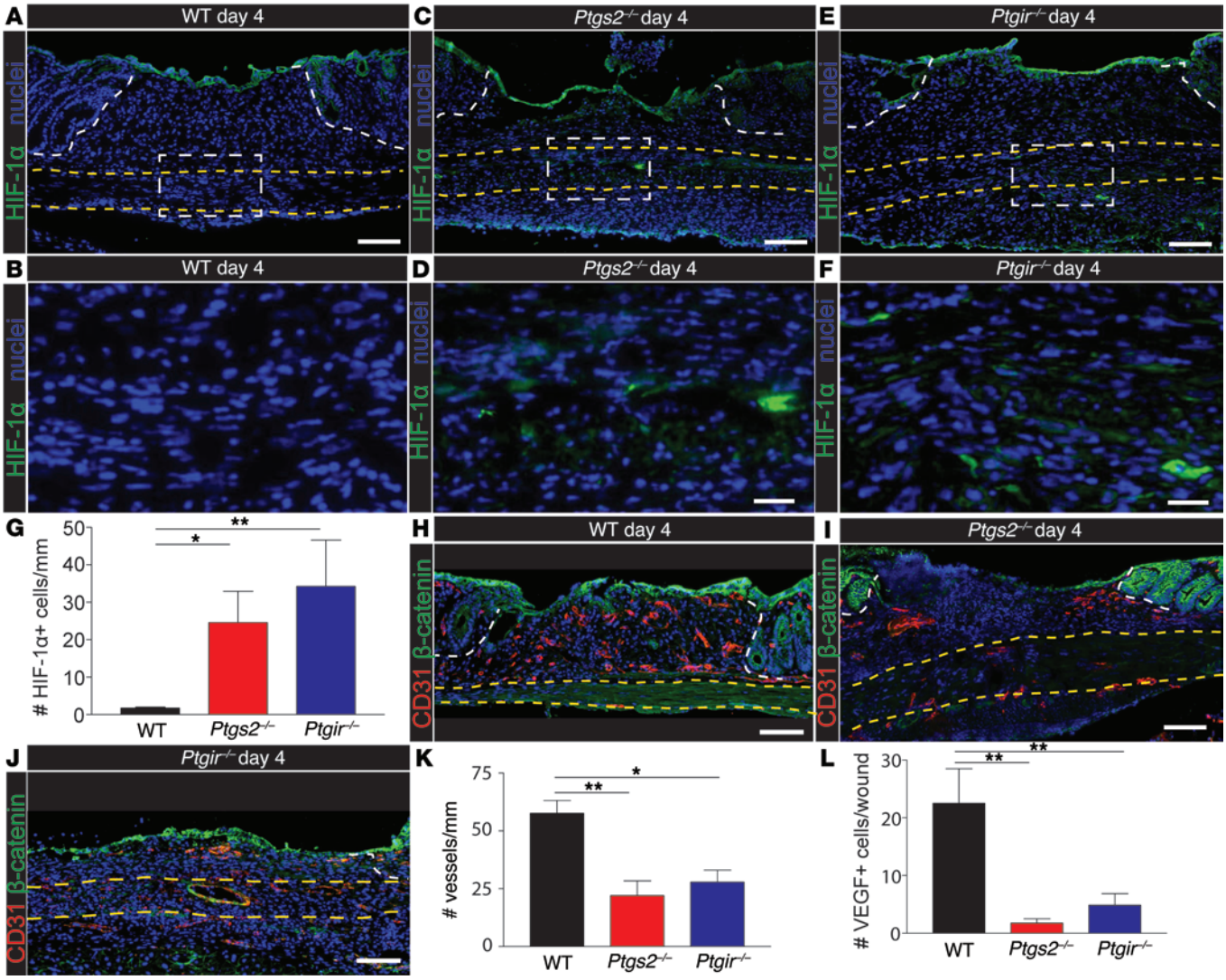

Figure 3. *Ptgs2*$^{-/-}$ and *Ptgir*$^{-/-}$ mice have hypoxia and defective angiogenesis after mucosal injury. (**A**–**F**) Representative images of colons (3 mice per group in 3 experiments) from (**A**) WT (n = 7 wounds), (**C**) *Ptgs2*$^{-/-}$ (n = 5 wounds), and (**E**) *Ptgir*$^{-/-}$ (n = 5 wounds) mice 4 days after injury stained with anti–HIF-1α antisera (green, hypoxic cells) and bisbenzimide (blue, nuclei). Dashed white lines outline wound beds, dashed yellow lines outline muscularis propria, and dashed white boxes indicate the areas shown at higher magnification in **B**, **D**, and **F**. (**G**) Number of HIF-1α–positive cells per wound bed length (n = 5–7 wounds per group). P = 0.0056, 1-way ANOVA; P < 0.001, Bartlett's test for unequal variance. (**H**–**J**) Representative images of colons (n = 5–6 wounds per group from 3 mice per group in 3 experiments) from (**H**) WT (n = 5 wounds), (**I**) *Ptgs2*$^{-/-}$ (n = 6 wounds), and (**J**) *Ptgir*$^{-/-}$ (n = 5 wounds) mice 4 days after colonic biopsy injury stained with anti-CD31 (red, blood vessels) and anti–β-catenin antisera (green, epithelium). (**K**) Number of blood vessels found in the wound bed divided by the width of the wound bed in indicated groups of mice 4 days after injury (n = 5–6 wounds per group). P = 0.0038, 1-way ANOVA. (**L**) Number of VEGF-positive cells per wound bed from WT (n = 5 wounds), *Ptgs2*$^{-/-}$ (n = 5 wounds), and *Ptgir*$^{-/-}$ (n = 7 wounds) mice. n = 5–7 wounds per group from 3 mice per group in 3 experiments. P = 0.0013, 1-way ANOVA; P = 0.0021, Bartlett's test for unequal variance. *P < 0.05, **P < 0.01, Tukey's post-test. Scale bar: 100 μm (**A**, **C**, **E,** and **H**–**J**); 25 μm (**B**, **D**, and **F**). Mean ± SEM.

how penetrating ulcers form, we were able to investigate whether transplanted MSCs could be a potential therapy to stimulate intestinal repair in our model. We hypothesized that MSCs could be a potential cellular therapy because they express high levels of VEGF in culture relative to other growth factors and cytokines (33). We chose to use MSCs isolated from the colon in our studies because they have higher levels of VEGF expression as compared with MSCs isolated from the bone marrow (34).

A major technical challenge in using MSCs for the treatment of intestinal diseases is the route of delivery. As the majority of clinical trials use intravenous delivery, we initially intravenously injected 1×10^6 cMSCs that were isolated from the colons of GFP-expressing mice. Cells were injected 24 hours after colonic biopsy injury into *Ptgir*$^{-/-}$ mice. We found no detectable GFP-expressing cells in wound beds 5 days after transplantation (Figure 5A). After intravenous injection, the majority of monolayer-cultured MSCs typically become trapped in the lung (5), in which they can potentially exert systemic effects by secretion of antiinflammatory factors acting at long distances (35). However, biopsy-injured *Ptgir*$^{-/-}$ mice given intravenous cMSCs still had marked smooth muscle necrosis in areas of colonic injury (Figure 5B).

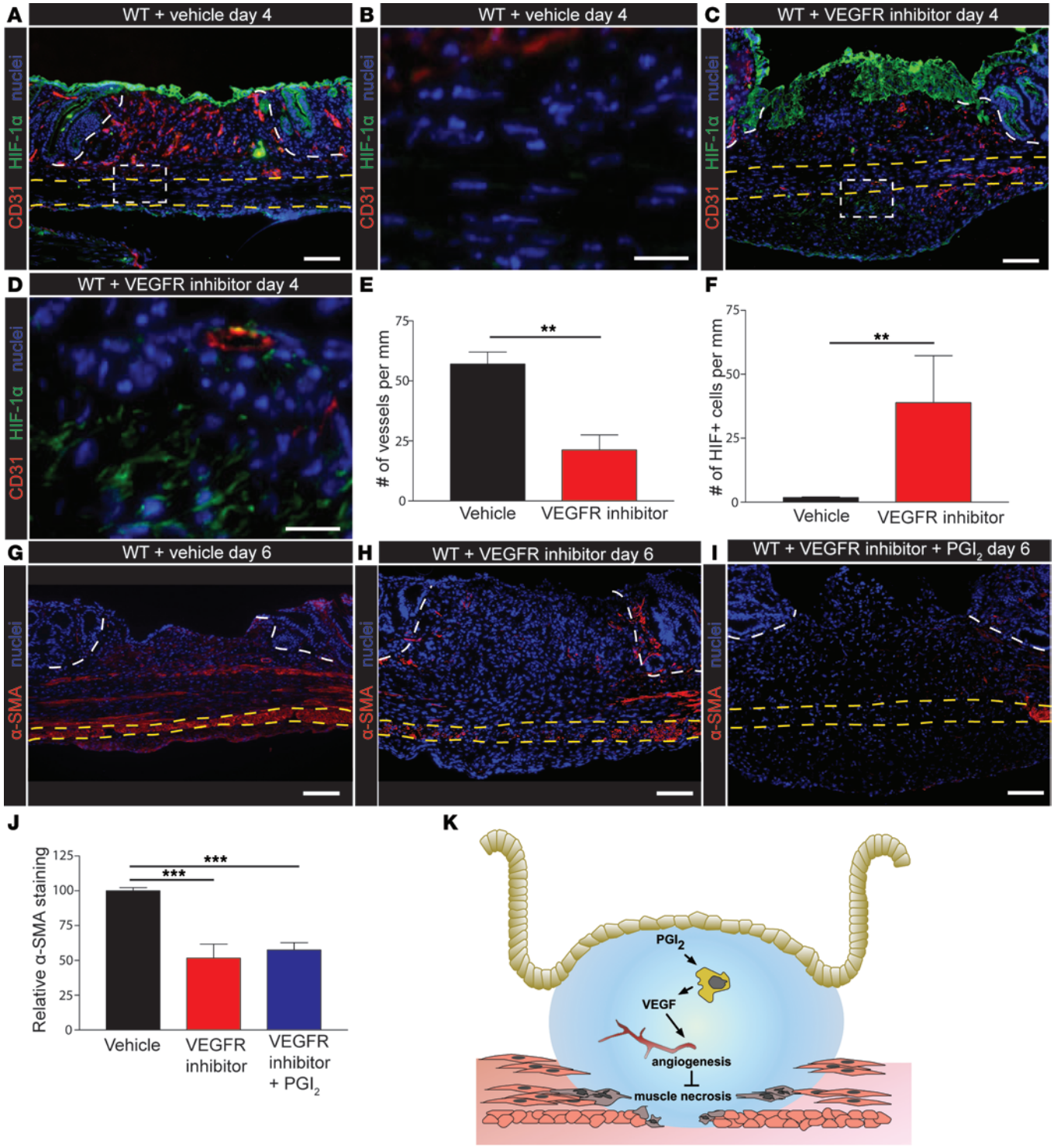

Figure 4. VEGFR inhibition leads to defective angiogenesis and penetrating ulcers after mucosal injury. (**A–D**) Representative images of colonic sections (n = 5 wounds per group from 3 mice per group in 3 experiments) 4 days after injury from WT mice treated with (**A**) vehicle or (**C**) VEGFR inhibitor tivozanib. Sections were stained with anti-CD31 antisera (red, blood vessels), anti–HIF-1α antisera (green, hypoxic cells), and bisbenzimide (blue, nuclei). Dashed white lines outline wound beds, dashed yellow lines outline the muscularis propria, and dashed white boxes indicate the areas shown at higher magnification in **B** and **D**. (**E**) Number of blood vessels within the wound bed per wound bed length in vehicle-treated and tivozanib-treated mice. n = 5 wounds per group from 3 mice per group in 3 experiments. $^{**}P < 0.01$, Student's t test. (**F**) Number of HIF-1α–positive cells per wound bed length in vehicle-treated and tivozanib-treated mice. $^{**}P < 0.01$, Mann-Whitney test. (**G–I**) Representative images of colonic sections (3–4 mice per groups in 3 experiments) from WT mice given (**G**) vehicle (n = 6 wounds from 3 mice), (**H**) tivozanib (n = 6 wounds from 3 mice), or (**I**) tivozanib and PGI_2 analog (n = 9 wounds from 4 mice) 6 days after injury stained with anti–α-SMA antibodies (red, smooth muscle) and bisbenzimide (blue, nuclei). (**J**) Relative α-SMA staining of the outer muscle layer in indicated groups of mice 6 days after injury. n = 6–9 wounds per group from 3–4 mice per group in 3 experiments. $P = 0.0001$, 1-way ANOVA. $^{***}P < 0.001$, Tukey's post-test. (**K**) Schematic depicting the model of penetrating ulcer formation. PGI_2 stimulates VEGF production in the wound bed, which stimulates angiogenesis and prevents muscle necrosis. Scale bar: 100 μm (**A**, **C**, and **G–I**); 25 μm (**B** and **D**). Mean ± SEM.

We hypothesized that transplanted cMSCs must be located in the wound bed to stimulate angiogenesis because VEGF has a short half-life in serum (~20–30 minutes) (36). Therefore, we developed what we believe to be a novel technique to inject cMSCs directly into the intestinal mucosa. We injected 1×10^6 GFP-expressing cMSCs under endoscopic guidance into the submucosa just proximal to the anorectal junction 24 hours after *Ptgir*$^{-/-}$ mice were injured via biopsy (Supplemental Figure 13). We found that within 5 days cMSCs migrated to all wound beds within the distal colon (Figure 5C and Supplemental Figure 14) and rescued the muscle necrosis phenotype (Figure 5, D and E). In addition, the vascular pattern was rescued at day 4 after injury, and the numbers of VEGF-positive cells and blood vessels in *Ptgir*$^{-/-}$ mice were similar to those in WT mice (Figure 5, F–H, and Supplemental Figure 15). Furthermore, we did not find any evidence of cMSC differentiation into endothelial cells or smooth muscle cells by 6 days after injury (Supplemental Figure 16). These findings suggested that mucosally injected cMSCs migrated to the wound bed and stimulated angiogenesis and thus prevented smooth muscle necrosis.

To confirm that mucosally transplanted cMSCs must migrate to wound beds to stimulate repair, we tested a known inhibitor of MSC chemotaxis. The best-characterized receptor on MSCs that responds to chemotactic factors is CXCR4 (37, 38). We treated *Ptgir*$^{-/-}$ mice injected with 1×10^6 GFP-expressing cMSCs with AMD3100, a well-established inhibitor of CXCR4 (39). Inhibition of CXCR4 was sufficient to block the migration of cMSCs into the wound bed as compared with that in controls (Figure 5I). The majority of the transplanted cMSCs remained at the injection site in these mice (Figure 5J). Importantly, AMD3100-treated *Ptgir*$^{-/-}$ mice showed smooth muscle necrosis, indicating that cMSCs must act locally within the wound bed (Figure 5, K and L). Taken together, our results support the hypothesis that cMSCs produced VEGF locally to stimulate angiogenesis and prevent muscle necrosis in *Ptgir*$^{-/-}$ mice.

cMSCs required maximal VEGF expression to rescue smooth muscle necrosis. To test that VEGF expression in cMSCs was a major factor that stimulated angiogenesis and prevented muscle necrosis in injured mouse colons, we performed knockdown of VEGF expression in cMSCs. We produced two separate lines using independent shRNAs that showed a 55% and 75% reduction of *Vegf* mRNA as compared with nontargeting shRNA lines (Figure 6A). This level of knockdown is relevant, as mice that are heterozygous for *Vegf* are not viable due to the exquisite dose dependency of VEGF (29). Nontargeting and VEGF shRNA lines maintained cell surface markers consistent with those of cMSCs (Supplemental Figure 17) (34). We found that the minimal number of nontargeting shRNA cMSCs that rescued muscle necrosis in injured *Ptgir*$^{-/-}$ mice was 3×10^5 injected cells (Figure 6B). We injected the two VEGF knockdown lines at this dose and found that they were less effective at preventing muscle necrosis in injured *Ptgir*$^{-/-}$ mice (Figure 6, C and D). We then surmised that injecting greater numbers of VEGF knockdown cells should increase VEGF delivery and also rescue smooth cell necrosis. We found that, at the dose of 1×10^6 injected cells, both the scrambled and VEGF shRNA cells rescued smooth muscle loss (Supplemental Figure 18). These results support a critical role of VEGF in preventing muscle necrosis in areas immediately beneath mucosal wounds.

Discussion

The penetrating ulcers in biopsy-injured *Ptgs2*$^{-/-}$ mice model penetrating ulcers that can develop in patients with inflammatory bowel disease or in patients taking chronic NSAIDs or VEGF inhibitors (15, 22). We took an in vivo approach to explain the mechanism of penetrating ulcer formation in our model. Mucosal injury in *Ptgs2*$^{-/-}$ mice caused smooth muscle necrosis in areas directly underlying the injury that was secondary to hypoxic injury and poor angiogenic response in the wound bed. We found that PGI_2 stimulated VEGF expression and angiogenesis within wound beds. We then developed a method to mucosally inject cMSCs in order to deliver VEGF to colonic wounds. We found that mucosally injected cMSCs were better able to migrate to wounds than intravenously injected cMSCs and were recruited in a CXCR4-dependent mechanism. Mucosally injected cMSCs rescued defects in repair, which was dependent on VEGF expression and stimulation of angiogenesis in the wound bed (Figure 6E).

Our results have potential clinical relevance for the prevention and treatment of penetrating ulcers that occur as a complication of gastrointestinal diseases. For example, local injection of MSCs is being tested as a treatment for perianal fistulas associated with Crohn's disease (40). Perianal fistula formation is a common complication of Crohn's disease, with a risk for development of between 17% and 50% (41). In phase I (42) and phase II (43) clinical trials by the same group, MSCs injected into fistulas led to improved healing. Although MSCs are an exciting potential treatment for perianal fistulas, more research is needed to determine their mechanism of action and optimal conditions for use. Based on our results, we would propose that local angiogenesis is an important mechanism.

Future studies should also consider comparing MSCs isolated from different tissues and different methods of in vitro expansion. The purpose would be to find and utilize MSCs with the highest VEGF expression. For example, global gene analysis of MSCs isolated from mice showed that cMSCs produce more *Vegf* mRNA than bone marrow MSCs (34). It is likely that cMSCs produce other proangiogenic or prohealing factors that work via other pathways, but our results suggest that MSCs are most effective for mucosal wound healing when injected intramucosally and that VEGF expression/angiogenesis plays an important part in mucosal repair.

MSCs are also being tested for treatment of Crohn's disease due to their antiinflammatory properties, though the early clinical trials have been inconclusive (44), possibly due to the use of intravenous delivery of MSCs. Our results are consistent with the predominant theory that intravenous transplantation leads to the majority of MSCs getting trapped in the lung and poor recruitment to inflamed or injured peripheral tissues (4). As such, we suggest that mucosal injection into the rectum just proximal to the anorectal junction may allow MSCs to migrate more successfully throughout the inflamed intestine and may lead to improved regeneration and mucosal healing in patients with Crohn's disease.

Our results suggest that poor angiogenic response after mucosal injury is a common mechanism that can lead to penetrating ulcers in mice and humans. We found that tivozanib, which selectively inhibits the 3 VEGF receptors and potently inhibits angiogenesis in vivo (31, 45), caused penetrating ulcers similar

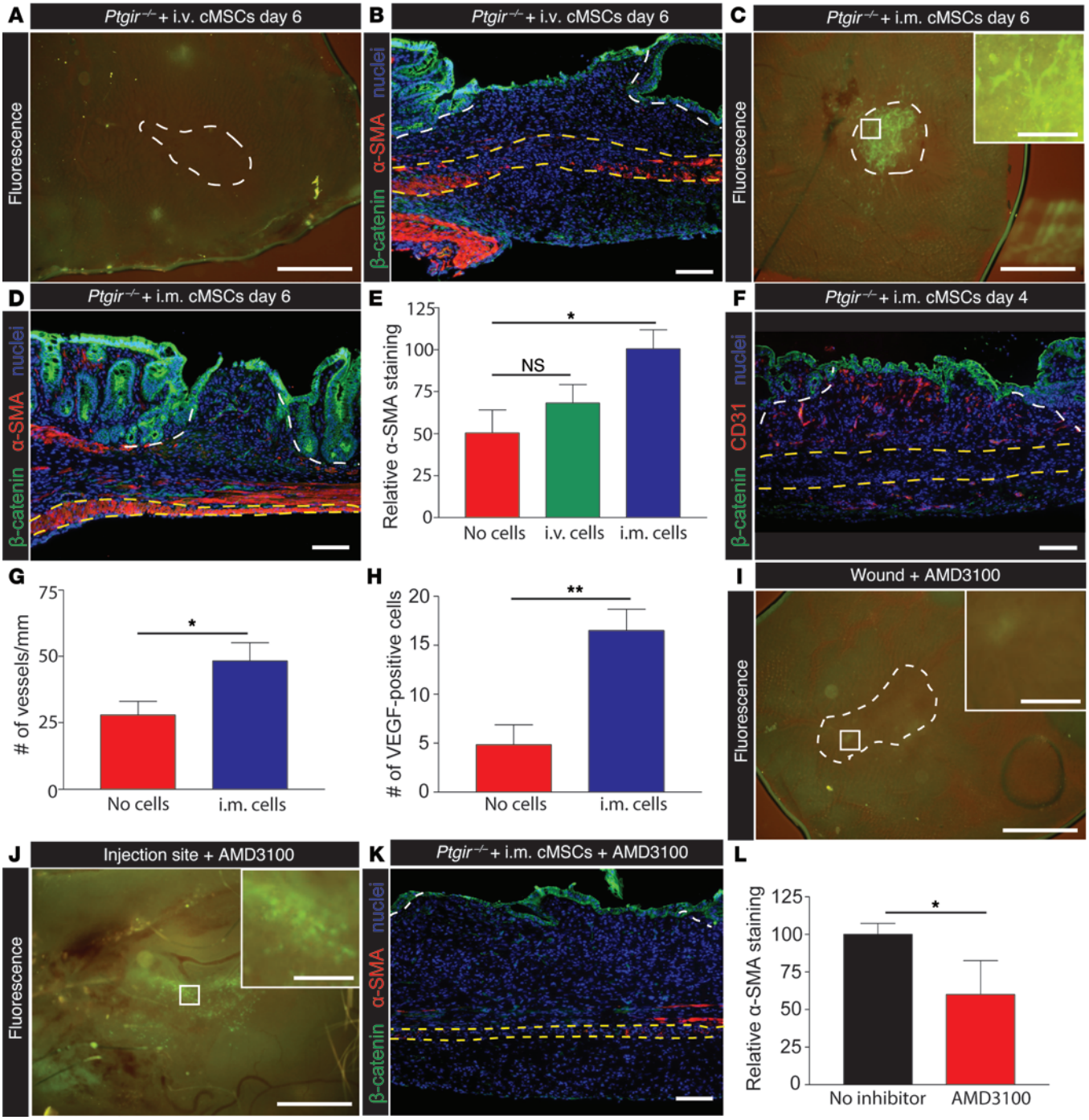

Figure 5. Mucosally injected cMSCs migrate to wounds and prevent penetrating ulcers in injured *Ptgir*$^{-/-}$ mice. (**A** and **C**) Fluorescent image of *Ptgir*$^{-/-}$ wound 5 days after (**A**) intravenous or (**C**) mucosal injection of GFP-expressing cMSCs (n = 8 wounds from 4 mice in 4 experiments). (**B**) Section from **A** and (**D**) from **C** stained with β-catenin and α-SMA antisera. (**E**) Relative α-SMA staining in the outer muscle layer underlying wounds from indicated groups of mice. P = 0.0159, 1-way ANOVA. *P < 0.05, Tukey's post-test. n = 8 wounds per group. (**F**) Colon section (n = 6 wounds from 3 mice in 3 experiments) from *Ptgir*$^{-/-}$ mice 3 days after intramucosal cMSC injection stained with CD31 and β-catenin antisera. (**G**) Number of blood vessels per wound bed length and (**H**) number of VEGF-positive cells per wound bed 4 days after injury in *Ptgir*$^{-/-}$ or *Ptgir*$^{-/-}$ plus intramucosal cMSCs. *P < 0.05, **P < 0.01, Student's t test, n = 6 wounds per group. (**I** and **J**) Fluorescent image of (**I**) day 6 *Ptgir*$^{-/-}$ wound given intramucosal cMSCs and CXCR4 inhibitor AMD3100 (n = 6 wounds from 3 mice in 3 experiments) and (**J**) the injection site from mouse in **I**. (**K**) Section from **I** stained with β-catenin and α-SMA antisera. (**L**) Relative α-SMA staining in the outer muscle layer underlying *Ptgir*$^{-/-}$ wounds (n = 6–10 wounds per group). *P < 0.05, Student's t test. White boxes indicate areas shown at high magnification. Scale bar: 1 mm (**A**, **C**, **I,** and **J**); 100 μm (**B**, **D**, **F**, and **K**); 125 μm (**C**, inset; **I**, inset; and **J**, inset). Mean ± SEM.

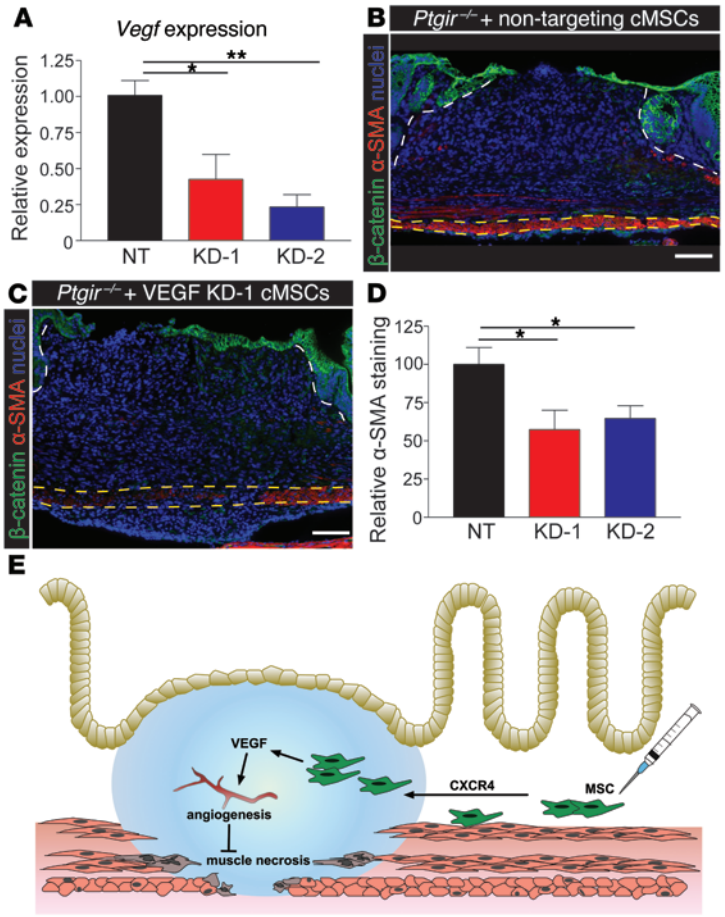

Figure 6. cMSCs require VEGF expression to prevent penetrating ulcers in injured *Ptgir*$^{-/-}$ mice. (**A**) Relative expression of *Vegf* mRNA in cMSCs that contain nontargeting (NT) or VEGF knockdown shRNA (two separate clones KD-1 and KD-2). $P = 0.0081$, 1-way ANOVA. $^{*}P < 0.05$, $^{**}P < 0.01$, Tukey's post-test. $n = 3$ biological replicates plated at 3 sequential passages per group, repeated in technical triplicates. (**B** and **C**) Representative sections of colon ($n = 5$–6 wounds per group from 3 mice per group in 3 experiments) from a *Ptgir*$^{-/-}$ mouse 6 days after injury and (**B**) 5 days after mucosal injection of nontargeting cMSCs or (**C**) VEGF knockdown line KD-1 stained with anti–β-catenin antisera (green, epithelium), anti–α-SMA antisera (red, smooth muscle cells), and bisbenzimide (blue, nuclei). (**D**) Relative α-SMA staining in the outer muscle layer underlying wounds from *Ptgir*$^{-/-}$ mice injected with nontargeting ($n = 5$ wounds from 3 mice), KD-1 ($n = 6$ wounds from 3 mice), or KD-2 ($n = 10$ wounds from 4 mice) cMSCs in 3 experiments. $P = 0.0265$, 1-way ANOVA. $^{*}P < 0.05$, Tukey's post-test. (**E**) Schematic depicting how transplanted cMSCs stimulate repair. Intramucosally transplanted cMSCs can migrate to wounds in a CXCR4-dependent manner. Once cMSCs enter wounds, they provide VEGF to stimulate angiogenesis and prevent smooth muscle necrosis. Scale bar: 100 μm. Mean ± SEM.

to those in injured *Ptgs2*$^{-/-}$ mice. Interestingly, similar to chronic NSAID use, VEGF inhibitors are associated with human gastrointestinal perforations. The anti-VEGF antibody bevacizumab is associated with bowel perforation in up to 2.4% of patients with cancer, through unknown mechanisms (46). Penetrating ulcer and fistula formation also occurs in patients with inflammatory bowel disease, who have been shown to have abnormal blood vessel architecture and angiogenic responses due to chronic inflammation (47). We suggest that hypoxia and subsequent necrosis occur secondarily to defective angiogenesis, which may be a common mechanism for development of penetrating ulceration in humans.

We previously showed that *Ptgs2*$^{-/-}$ mice lost α-SMA staining underlying wound beds at day 6 after injury (14). As α-SMA expression can be downregulated in myofibroblasts (48) or vascular cells (49) following inflammation, it is possible that smooth muscle cells in injured *Ptgs2*$^{-/-}$ mice underwent dedifferentiation following injury. We tracked marked smooth muscle cells using injured *Acta2-CreER*^{T} *R26*$^{mT/mG}$ mice in which tamoxifen injection efficiently marked all α-SMA–expressing cells before injury. This model allowed us to determine that cells in the muscularis propria did not downregulate α-SMA in PTGS2-inhibited mice 6 days after injury and instead led to smooth muscle cell death.

One unexpected finding was that PGI_2 was the critical prostaglandin to stimulate angiogenesis and prevent penetrating ulcers after colonic biopsy injury. PGE_2 has been shown to stimulate angiogenesis in many models and induce VEGF expression in several cell types in vitro (19, 50, 51). In contrast, PGI_2 has been relatively understudied in vivo. A few studies suggest that PGI_2 is potentially relevant, as it can induce VEGF in several cell types known to be important in mucosal wounds, including fibroblasts (52) and macrophages (53). The PGE_2 analog used in this study does not bind one of the PGE_2 receptors, EP1, and the PGI_2 analog used in this study can activate EP1 (54–56). Therefore, it is possible that EP1 signaling, in addition to PGI_2 receptor signaling, could play a role in preventing smooth muscle loss. However, our genetic knockout studies found a clear role for PGI_2 and its downstream receptor in the prevention of penetrating ulcers in the colon through stimulation of angiogenesis.

Here, we have shown that transplanted cMSCs can stimulate proper repair using a mouse model of penetrating ulcers in the gastrointestinal tract. Few studies have determined the mechanisms by which transplanted MSCs ameliorate disease. One such study showed that intravenously transplanted MSCs became trapped in the lung and secreted TSG-6, which systemically dampened inflammation and reduced myocardial infarction size (35). We describe in detail one disease condition in which MSCs must migrate locally to modulate the injured tissue microenvironment. The major difference in our mechanism is that VEGF does not have a long half-life and must be produced near the injured tissue. We anticipate that these findings will be translated to human gastrointestinal disorders, such as inflammatory bowel disease, and may have relevance for chronic tissue injury and repair outside of the gastrointestinal tract.

Methods

Generation of the *Acta2-CreER*^{T} line

The *Acta2-CreER*^{T} line was generated using the same method as described in earlier reports (57). Briefly, the *Acta2*-containing BAC clone (RP24-374H8) was purchased from the Children's Hospital Oakland Research Institute. The BAC was isolated and transformed

into SW105-competent cells. A CreERT FrtNeoFrt cassette was PCR amplified from a pl451 plasmid with primer overhangs homologous to the sequence surrounding the ATG translational start site of *Acta2*. The PCR product was inserted into the BAC using recombineering. After removal of the Neo cassette by arabinose-induced flippase, BAC DNA was microinjected into the pronucleus of fertilized CBAx-C57BL/6J oocytes. Only 1 of 2 positive potential founders transmitted through the germline to F_1. This line 1 was backcrossed to C57BL/6J for at least 6 generations and was used for all subsequent experiments. Genotyping for *Acta2-CreER^T* was done using forward primer 5′-ACCAAGAACCCTGTCTGTGG-3′ and reverse primer 5′-CATGTTTAGCTGGCCCAAAT-3′.

Mice

Ptgs2$^{+/-}$ mice (58) were bred to generate littermate WT, *Ptgs2$^{+/-}$*, and *Ptgs2$^{-/-}$* progeny for experiments. *Ptgir$^{+/-}$* mice (23) were a gift from Gregg Rokosh (University of Louisville, Louisville, Kentucky, USA) and were bred to generate WT, *Ptgir$^{+/-}$*, and *Ptgir$^{-/-}$* mice. *Acta2-CreER^T* mice were crossed with *R26$^{mT/mG}$* reporter mice (24) to label smooth muscle cells with EGFP. CMV immediate enhancer/β-actin promoter GFP mice (with global GFP expression) were obtained from The Jackson Laboratory. All mice were obtained from breeding colonies in the same barrier facility Clinical Sciences Research Building, Washington University Medical Center. All mice were on a C57BL/6 background, and adult male and female mice were used at between 8 to 16 weeks of age.

Mouse colonic biopsy method

We used a high-resolution miniaturized colonoscope system (Karl Storz) to visualize the colons in 10- to 16-week-old anesthetized mice (14). We inflated the colons with PBS and removed fecal pellets using suction to allow for clear visualization of the distal colon by the endoscope. We then removed 1 to 3 full-thickness areas per mouse using 3 French flexible biopsy forceps inserted into the sheath adjacent to the camera. These biopsy injuries included the mucosa and submucosa and were spaced approximately 1 cm apart along the dorsal side of the colon of each mouse. Biopsy injuries were performed up to 6 cm from the anorectal junction and could not be performed past the transverse colon because of the rigid endoscope. All genetically modified mice were injured with the same technique. The inclusion criteria for a given wound were that there was no initial penetration of the muscularis propria (leading to an immediate perforation) and that the wound size was approximately 1 mm^2, which is equivalent to removal of approximately 250 to 300 crypts.

Smooth muscle–tracing experiments

Acta2-CreER^T R26$^{mT/mG}$ mice were injected i.p. with 4 mg tamoxifen (Toronto Research Chemicals) 2 weeks before colonic biopsy. The reporter mouse expresses membrane-tethered tdTomato in all cells (driven by the ROS26 locus) (24). Activation of Cre recombinase in the *Acta2*-expressing cells eliminates tdTomato expression and switches on EGFP in these cells. When we stained for α-SMA, tdTomato could not be detected due to the high relative signal of α-SMA.

After colonic biopsy, mice were given daily i.p. injections of 5 mg/kg NS-398 (Cayman Chemical) or DMSO vehicle until sacrifice at day 6. A 25 mg/ml stock solution (in DMSO) was diluted to 5 mg/kg in sterile saline for daily injections. A volume of 150 μl was used for each injection.

Colonic processing for wound sections

Mice were sacrificed 2, 4, or 6 days after colonic biopsy. The dissected colons were flushed with PBS and then OCT compound and opened longitudinally. The wound beds, including 1 to 2 mm of adjacent uninjured area, were pinned out and cut with a razor blade under guidance of a stereoscope (Olympus) and photographed (Olympus). Then, 10- × 10-mm fragments of intestine, with the wound located at the center, were frozen in OCT, and perpendicular serial 5-μm sections were cut completely through each wound bed in a proximal to distal orientation relative to the in vivo colon (see ref. 14 for additional details). The sections from the center of the wound were used for analysis and stored at –80°C until use.

Immunofluorescence staining of wound sections

Stored frozen sections of colons were immediately fixed in 4% paraformaldehyde (in PBS, pH 7.4) for 10 minutes at 4°C, rinsed in PBS (three 5-minute washes) at 24°C, blocked in 3% bovine serum albumin/0.5% Triton-X for 20 minutes at 24°C, and incubated with primary antibody for 1 hour at 24°C. Sections were then rinsed 3 times for 5 minutes each time with PBS and incubated with secondary antibodies for all nonconjugated primary antibodies for 1 hour at 24°C. Sections were then rinsed 3 times for 5 minutes each time with PBS, stained with bisbenzimide (1:10,000 dilution, Life Technologies) to label nuclei, and mounted with Mowiol 4-88 (EMD Chemicals). Sections were photographed with a Zeiss Axiovert 200 with an Axiocam MRM camera.

Antibodies for immunofluorescence and flow cytometry

Primary antibodies used were mouse monoclonal anti–α-SMA conjugated to Cy3 (clone 1A4; Sigma-Aldrich), rat monoclonal anti-EpCAM conjugated to Alexa Fluor 647 (clone G8.8; BioLegend), rabbit monoclonal anti-Ki67 (clone SP6; Vector), rat monoclonal anti-CD29 (clone KMI6; BD Biosciences), rat monoclonal anti-CD31 (clone MEC 13.3; BD Biosciences), rat monoclonal anti-CD44 (clone IM7; BD Biosciences), rat monoclonal anti-CD45 (clone 30-F11; BD Biosciences), rat monoclonal IgG2a isotype control (clone R11-89; BD Biosciences), rat monoclonal IgG2b isotype control (clone RTK4530; BD Biosciences), rabbit polyclonal anti–HIF-1α (Novus), rabbit polyclonal anti–β-catenin (Sigma-Aldrich), rat monoclonal anti-VEGF (clone 1F07-2C01; BioLegend), rat polyclonal anti-GFP (Abcam), rat monoclonal anti-F4/80 conjugated to Alexa Fluor 488 (clone BM8; BioLegend), rabbit monoclonal anti–cleaved caspase-3 (clone 5A1E; Cell Signaling Technology), and mouse monoclonal anti–EF5 (clone ELK3-51 conjugated to Alexa Fluor 488; gift provided by Cameron Koch, University of Pennsylvania, Philadelphia, Pennsylvania, USA). All primary antibodies were used at 1:100 except for anti-VEGF (1:50), anti-Ki67 (1:200), anti–α-SMA (1:500), and anti–EF5 (provided at 75 μg/ml concentration and not diluted). For all unconjugated antibodies, appropriate donkey anti-rat or anti-rabbit secondary antibodies conjugated to Alexa Fluor 488 or Alexa Fluor 594 (Life Technologies) were used at 1:500 dilution to visualize staining.

Quantification of immunofluorescence images

α-SMA. Colonic sections stained with anti–α-SMA-Cy3 antisera were photographed at 10×, and the images were cropped to only include the wound bed and underlying muscle layers. The Cy3 channel was opened in ImageJ software (http://imagej.nih.gov/ij/), converted to binary, and the outer longitudinal muscle was outlined by hand. The average

number of α-SMA–positive pixels per wound bed length was calculated for each outlined area. This process was repeated 5 times per wound, and an average value was recorded. Each average value was normalized to WT or control wounds and reported as a percentage.

HIF-1α– and EF5-positive cells. Colonic sections stained with HIF-1α and EF5 antisera were photographed at 10×, which included the entire wound bed. The number of positive staining cells within the wound bed or muscle layers was divided by the total wound bed length. We used the detectable HIF-1α staining in surface epithelial cells as the threshold to enumerate HIF-1α–positive cells in the wound bed.

Blood vessels. Colonic sections stained with anti-CD31 antisera were photographed at 10×, which included the entire wound bed. The number of detectable $CD31^+$ clusters within the wound bed was divided by the total wound bed length.

VEGF-positive cells. Overlapping images of the wound bed were taken at high magnification (×40). A construct of the entire wound bed was produced, and the total number of VEGF-positive cells was recorded per wound bed.

Inhibitors and compounds

The 2-nitroimidazole compound EF5 was a gift from Cameron Koch (University of Pennsylvania) produced by the National Cancer Institute. EF5 was dissolved in ethanol and then diluted in glucose to yield a final concentration of 10 mM EF5 in 5% glucose/2.4% ethanol solution 5% glucose plus 2.4% ethanol. We i.p. injected 10 μl/g body weight of the 10 mM drug solution 2 hours before sacrifice (1% by body weight). Staining specificity was tested by using the anti-EF5 antibody (regular stain) or anti-EF5 antibody mixed with 0.5 mM EF5 (competed stain) on serial sections.

The pan-VEGFR inhibitor tivozanib (AV-951; AdooQ BioScience) was dissolved in DMSO to produce a 20 mg/ml stock solution. Tivozanib (1 μg/kg body weight) was diluted into 300 μl corn oil and orally gavaged into WT mice once daily.

The selective PTGS2 inhibitor NS-398 (Cayman Chemical) was dissolved in DMSO to produce a 25 mg/ml stock solution. NS-398 was then diluted in sterile saline each day and i.p. injected at 5 mg/kg mouse body weight.

The PGE_2 analog 16,16-dimethyl prostaglandin E2 (Cayman Chemical) and PGI_2 analog iloprost (Cayman Chemical) were diluted into sterile 5% sodium bicarbonate immediate before use. Iloprost (200 μg/kg body weight) or 16,16-dimethyl prostaglandin E2 (10 μg/kg or 100 μg/kg body weight) were injected i.p. twice daily into biopsy-injured *Ptgs2*$^{-/-}$ mice.

The CXCR4 inhibitor AMD3100 (Sigma-Aldrich) was dissolved in water and i.p. injected once daily at 10 mg/kg body weight in sterile saline.

Immunoblotting for necroptosis

Extracts of whole colonic tissue (2 mm × 2 mm) were made by homogenization at 4°C in RIPA buffer containing NaF (50 mM), phosphatase inhibitors (no. 2 and 3; Sigma-Aldrich), and a protease inhibitor cocktail (Sigma-Aldrich). After centrifugation, supernatants were mixed with a loading buffer containing DTT (100 mM) and boiled, and 15 μg protein was loaded onto a 4% to 15% polyacrylamide gel. After gel electrophoresis and transfer to PVDF membrane, blots were blocked and stained overnight at 4°C with a rabbit monoclonal antibody against mouse phospho-MLKL (Abcam) or a mouse monoclonal antibody against mouse β-actin (Sigma-Aldrich), followed by detection with HRP-labeled secondary anti-IgG antibodies and visualization by chemiluminescence (SuperSignal West Pico, Thermo Scientific Pierce).

Isolation of cMSCs

cMSCs were isolated from WT or CMV immediate enhancer/β-actin promoter GFP mice (The Jackson Laboratory) using a protocol adapted from a previous study (34). Briefly, the colons were removed, flushed, minced, and treated with media containing 1 mM DTT for 20 minutes to remove epithelial cells. The tissue was then treated with 0.66 mg/ml collagenase type 1 (from *Clostridium histolyticum*; Life Technologies) for 45 minutes in a shaking incubator at 37°C. Finally, the cells were filtered through a 70-μm filter, washed, plated on petri dishes, and allowed to attach overnight. Media containing Gibco Low-Glucose DMEM (Life Technologies) with 10 mmol/l HEPES and 10% FBS (Sigma-Aldrich) was changed every 2 to 3 days, and cMSCs grew out within a week. All experiments were performed using cells passaged fewer than 10 times after shRNA treatment.

Injection of cMSCs

For intravenous injection of cMSCs, 1×10^6 GFP-expressing cMSCs in 200 μl saline were injected into the tail veins of mice as slowly as possible 24 hours after biopsy injury. To setup the apparatus for mucosal injection of cells, a 30-gauge needle was attached using superglue to one end of an approximately 15-cm long piece of 26-gauge polytetrafluoroethylene thin-wall tubing (Zeus Industrial Products) each time an injection was performed. The tubing was inserted through the sheath adjacent to the colonoscope camera, and a 25-gauge needle was attached to the other end of the tubing that remained outside of the colonoscope. We then attached a syringe containing 1×10^6 GFP-expressing cMSCs in 100 μl of sterile saline to the needle outside of the colonoscope. 24 hours after biopsy, the 30-gauge needle was positioned just proximal to the anorectal junction and inserted at a minimal angle directly into the mucosa but not through the muscularis propria. cMSCs were then slowly injected into the mucosa to maintain cMSCs at the site of injection. Mice were sacrificed 5 days after cMSC injection, and the wounds were dissected, placed on a microscope slide, and observed under a fluorescent microscope to ensure that cMSCs successfully migrated into the wound beds up to 6 cm from the site of injection. For experiments using nontargeting or VEGF shRNA knockdown cMSCs, 3×10^5 cMSCs were injected just proximal to the anorectal junction 24 hours after injury, and mice were sacrificed at day 6 after injury. All wounds were then frozen in OCT and cut into 5-μm sections for analysis.

VEGF shRNA knockdown in cMSCs

VEGFA-targeted MISSION TRC2-pLKO shRNA plasmids (Sigma-Aldrich) or the MISSION SHC202 nontargeting control plasmid were transfected into 293FT cells (Life Technologies) along with psPAX2 packaging plasmid (a gift from Didier Trono, École Polytechnique Fédérale de Lausanne, Lausanne, Switzerland, Addgene plasmid 12260) and pMD2.G envelope plasmid (a gift from Didier Trono, Addgene plasmid 12259) using Lipofectamine 2000 reagent (Life Technologies) to generate shRNA-containing lentivirus. Lentiviral supernatant was harvested and concentrated with PEG-it Virus Precipitation Solution (System Biosciences) per vendor instructions. cMSCs isolated from WT mice were transduced at passage 5 by resus-

pending 8×10^4 cells in 100 μl lentiviral solution and incubated for 6 hours at 37°C. Cells were then washed and plated into a 24-well plate. Media were changed after 48 hours to media containing 5 μg/ml puromycin, and transduced MSCs were selected for 4 days. Remaining knockdown MSCs were maintained in media harvested from WT MSCs, filtered with a 0.2-μm syringe filter, and then mixed 1:1 with DMEM, 10 mmol/l HEPES, and 20% FBS. Cells were expanded at a ratio of no more than 2:1 to maintain sustainable density and assayed for *Vegf* gene expression after 3 to 5 passages after transduction. To measure *Vegf* mRNA in cMSCs, RNA was isolated by adding lysis buffer and using a NucleoSpin RNA Kit (Machery-Nagel). cDNAs were then synthesized using SuperScript III Reverse Transcriptase (Life Technologies), and quantitative RT-PCR was performed using SYBR Green Master Mix (Clontech Laboratories) on an Eppendorf RealPlex Mastercycler. The primer sequences were as follows: *Gapdh*, 5′-AGGTCGGTGTGAACGGATTTG-3′, 5′-TGTAGACCATGTAGTTGAGGTCA-3′; *Vegfa*, 5′-CTTGTTCAGAGCGGAGAAAGC-3′, 5′-ACATCTGCAAGTACGTTCGTT-3′.

Flow cytometry

cMSCs were resuspended in 100 μl FACS buffer (1% BSA in PBS) with the appropriate primary antibody for 30 minutes, washed twice with FACS buffer, resuspended in 100 μl FACS buffer with the appropriate secondary antibody for 30 minutes, washed again with FACS buffer, and analyzed on a FACSCalibur flow cytometer. All antibodies were used at 1:100 dilution. Analysis was performed using the FlowJo software.

Statistics

We performed all statistical analyses with Prism GraphPad 6.0. A *P* value of less than 0.05 was considered significant. Specific statistical tests are indicated in the figure legends. All tests were run with data from at least 5 wounds to give enough power for statistical tests. Student's *t* tests were 2 tailed. All parametric statistical tests meet the assumptions of the tests (normal distribution, equal variance) unless otherwise specified in the legends. Unequal variances of 1-way ANOVA were detected by Bartlett's test. Since all 1-way ANOVA tests were run with similar sample sizes, unequal variances were ignored, and the groups were considered different. Comparisons between 2 groups that did not meet the assumptions of a parametric *t* test were compared using the nonparametric Mann-Whitney test. Mice were randomly designated to control and treatment groups and were biopsy-injured in a blinded manner. Quantification of wound bed images was done in a blinded manner.

Study approval

All animal procedures were performed in accordance with the guidelines of the NIH. The generation of the *Acta2-CreER^T* line was approved by the Institutional Animal Care and Use Committee at Columbia University, New York, New York, USA. All other animal experiments were performed in accordance with approved protocols from the Washington University School of Medicine Animal Studies Committee.

Acknowledgments

We thank Ta-Chiang Liu, William Stenson, Kyunghee Choi, and Emil Unanue for careful reading of the manuscript and helpful comments throughout the study. We thank Hiroyuki Miyoshi for his expert advice and assistance throughout the study. We also thank the National Cancer Institute for providing EF5 and the labs of Sydney M. Evans and Cameron J. Koch in the Department of Radiation Oncology at the University of Pennsylvania School of Medicine for providing the anti-EF5 antisera, controls, and protocols. This work was supported by NIH grant DK07161907, NIH T32 HL007317 predoctoral training grant, and the Crohn's & Colitis Foundation of America Genetics Initiative. The Washington University Digestive Disease Research Core Center is supported by a grant from the National Institute of Diabetes and Digestive and Kidney Disease (P30DK052574).

Address correspondence to: Thaddeus S. Stappenbeck, Department of Pathology and Immunology, Washington University School of Medicine, Box 8118, 660 S. Euclid Avenue, St. Louis, Missouri 63110, USA. Phone: 314.362.4214; E-mail: stappenb@pathology.wustl.edu.

1. Almeida-Porada G, Soland M, Boura J, Porada CD. Regenerative medicine: prospects for the treatment of inflammatory bowel disease. *Regen Med*. 2013;8(5):631–644.
2. Voswinkel J, et al. Use of mesenchymal stem cells (MSC) in chronic inflammatory fistulizing and fibrotic diseases: a comprehensive review. *Clin Rev Allergy Immunol*. 2013;45(2):180–192.
3. Singer NG, Caplan AI. Mesenchymal stem cells: mechanisms of inflammation. *Annu Rev Pathol*. 2011;6:457–478.
4. Manieri NA, Stappenbeck TS. Mesenchymal stem cell therapy of intestinal disease: are their effects systemic or localized? *Curr Opin Gastroenterol*. 2011;27(2):119–124.
5. Fischer UM, et al. Pulmonary passage is a major obstacle for intravenous stem cell delivery: the pulmonary first-pass effect. *Stem Cells Dev*. 2009;18(5):683–692.
6. Zaher W, Harkness L, Jafari A, Kassem M. An update of human mesenchymal stem cell biology and their clinical uses. *Arch Toxicol*. 2014;88(5):1069–1082.
7. Glenn JD, Whartenby KA. Mesenchymal stem cells: Emerging mechanisms of immunomodulation and therapy. *World J Stem Cells*. 2014;6(5):526–539.
8. Leoni G, et al. Annexin A1, formyl peptide receptor, and NOX1 orchestrate epithelial repair. *J Clin Invest*. 2013;123(1):443–454.
9. Normand S, et al. Nod-like receptor pyrin domain-containing protein 6 (NLRP6) controls epithelial self-renewal and colorectal carcinogenesis upon injury. *Proc Natl Acad Sci U S A*. 2011;108(23):9601–9606.
10. Pickert G, et al. STAT3 links IL-22 signaling in intestinal epithelial cells to mucosal wound healing. *J Exp Med*. 2009;206(7):1465–1472.
11. Seno H, Miyoshi H, Brown SL, Geske MJ, Colonna M, Stappenbeck TS. Efficient colonic mucosal wound repair requires Trem2 signaling. *Proc Natl Acad Sci U S A*. 2009;106(1):256–261.
12. Miyoshi H, Ajima R, Luo CT, Yamaguchi TP, Stappenbeck TS. Wnt5a potentiates TGF-β signaling to promote colonic crypt regeneration after tissue injury. *Science*. 2012;338(6103):108–113.
13. Lee SJ, Leoni G, Neumann PA, Chun J, Nusrat A, Yun CC. Distinct phospholipase C-beta isozymes mediate lysophosphatidic acid receptor 1 effects on intestinal epithelial homeostasis and wound closure. *Mol Cell Biol*. 2013;33(10):2016–2028.
14. Manieri NA, Drylewicz MR, Miyoshi H, Stappenbeck TS. Igf2bp1 is required for full induction of *Ptgs2* mRNA in colonic mesenchymal stem cells in mice. *Gastroenterology*. 2012;143(1):110–121 e110.
15. Bataille F, et al. Morphological characterisation of Crohn's disease fistulae. *Gut*. 2004;53(9):1314–1321.
16. Molendijk I, Peeters KC, Baeten CI, Veenendaal RA, van der Meulen-de Jong AE. Improving the outcome of fistulising Crohn's disease. *Best Pract Res Clin Gastroenterol*. 2014;28(3):505–518.
17. Ballinger A. Adverse effects of nonsteroidal anti-inflammatory drugs on the colon. *Curr Gastroenterol Rep*. 2008;10(5):485–489.
18. Bjarnason I. Gastrointestinal safety of NSAIDs

and over-the-counter analgesics. *Int J Clin Pract*. 2013;(178):37–42.
19. Wang D, Mann JR, DuBois RN. The role of prostaglandins and other eicosanoids in the gastrointestinal tract. *Gastroenterology*. 2005;128(5):1445–1461.
20. Langman MJ, Morgan L, Worrall A. Use of anti-inflammatory drugs by patients admitted with small or large bowel perforations and haemorrhage. *Br Med J (Clin Res Ed)*. 1985;290:347–349.
21. Sostres C, Gargallo CJ, Lanas A. Nonsteroidal anti-inflammatory drugs and upper and lower gastrointestinal mucosal damage. *Arthritis Res Ther*. 2013;15(suppl 3):S3.
22. Tarnawski A, Szabo IL, Husain SS, Soreghan B. Regeneration of gastric mucosa during ulcer healing is triggered by growth factors and signal transduction pathways. *J Physiol Paris*. 2001;95(1-6):337–344.
23. Murata T, et al. Altered pain perception and inflammatory response in mice lacking prostacyclin receptor. *Nature*. 1997;388(6643):678–682.
24. Muzumdar MD, Tasic B, Miyamichi K, Li L, Luo L. A global double-fluorescent Cre reporter mouse. *Genesis*. 2007;45(9):593–605.
25. Masferrer JL, et al. Selective inhibition of inducible cyclooxygenase 2 in vivo is antiinflammatory and nonulcerogenic. *Proc Natl Acad Sci U S A*. 1994;91(8):3228–3232.
26. Nauta TD, van Hinsbergh VW, Koolwijk P. Hypoxic signaling during tissue repair and regenerative medicine. *Int J Mol Sci*. 2014;15(11):19791–19815.
27. Karhausen J, Furuta GT, Tomaszewski JE, Johnson RS, Colgan SP, Haase VH. Epithelial hypoxia-inducible factor-1 is protective in murine experimental colitis. *J Clin Invest*. 2004;114(8):1098–1106.
28. Koch CJ. Measurement of absolute oxygen levels in cells and tissues using oxygen sensors and 2-nitroimidazole EF5. *Methods Enzymol*. 2002;352:3–31.
29. Ferrara N, et al. Heterozygous embryonic lethality induced by targeted inactivation of the VEGF gene. *Nature*. 1996;380(6573):439–442.
30. Ben-Av P, Crofford LJ, Wilder RL, Hla T. Induction of vascular endothelial growth factor expression in synovial fibroblasts by prostaglandin E and interleukin-1: a potential mechanism for inflammatory angiogenesis. *FEBS Lett*. 1995;372(1):83–87.
31. De Luca A, Normanno N. Tivozanib, a pan-VEGFR tyrosine kinase inhibitor for the potential treatment of solid tumors. *IDrugs*. 2010;13(9):636–645.
32. Sun L, et al. Type I interferons link viral infection to enhanced epithelial turnover and repair. *Cell Host Microbe*. 2015;17(1):85–97.
33. Watanabe S, et al. Conditioned mesenchymal stem cells produce pleiotropic gut trophic factors. *J Gastroenterol*. 2014;49(2):270–282.
34. Walker MR, Brown SL, Riehl TE, Stenson WF, Stappenbeck TS. Growth factor regulation of prostaglandin-endoperoxide synthase 2 (Ptgs2) expression in colonic mesenchymal stem cells. *J Biol Chem*. 2010;285(7):5026–5039.
35. Lee RH, et al. Intravenous hMSCs improve myocardial infarction in mice because cells embolized in lung are activated to secrete the anti-inflammatory protein TSG-6. *Cell Stem Cell*. 2009;5(1):54–63.
36. Eppler SM, et al. A target-mediated model to describe the pharmacokinetics and hemodynamic effects of recombinant human vascular endothelial growth factor in humans. *Clin Pharmacol Ther*. 2002;72(1):20–32.
37. Wu Y, Zhao RC. The role of chemokines in mesenchymal stem cell homing to myocardium. *Stem Cell Rev*. 2012;8(1):243–250.
38. Marquez-Curtis LA, Janowska-Wieczorek A. Enhancing the migration ability of mesenchymal stromal cells by targeting the SDF-1/CXCR4 axis. *Biomed Res Int*. 2013;2013:561098.
39. Hummel S, Van Aken H, Zarbock A. Inhibitors of CXC chemokine receptor type 4: putative therapeutic approaches in inflammatory diseases. *Curr Opin Hematol*. 2014;21(1):29–36.
40. Voswinkel J, Francois S, Gorin NC, Chapel A. Gastro-intestinal autoimmunity: preclinical experiences and successful therapy of fistulizing bowel diseases and gut Graft versus host disease by mesenchymal stromal cells. *Immunol Res*. 2013;56(2–3):241–248.
41. Present DH. Crohn's fistula: current concepts in management. *Gastroenterology*. 2003;124(6):1629–1635.
42. Garcia-Olmo D, Garcia-Arranz M, Herreros D, Pascual I, Peiro C, Rodriguez-Montes JA. A phase I clinical trial of the treatment of Crohn's fistula by adipose mesenchymal stem cell transplantation. *Dis Colon Rectum*. 2005;48(7):1416–1423.
43. Garcia-Olmo D, et al. Expanded adipose-derived stem cells for the treatment of complex perianal fistula: a phase II clinical trial. *Dis Colon Rectum*. 2009;52(1):79–86.
44. Martinez-Montiel Mdel P, Gomez-Gomez GJ, Flores AI. Therapy with stem cells in inflammatory bowel disease. *World J Gastroenterol*. 2014;20(5):1211–1227.
45. Kang S, Roh YJ, Kim IB. Antiangiogenic effects of tivozanib, an oral VEGF receptor tyrosine kinase inhibitor, on experimental choroidal neovascularization in mice. *Exp Eye Res*. 2013;112:125–133.
46. Sliesoraitis S, Tawfik B. Bevacizumab-induced bowel perforation. *J Am Osteopath Assoc*. 2011;111(7):437–441.
47. Koutroubakis IE, Tsiolakidou G, Karmiris K, Kouroumalis EA. Role of angiogenesis in inflammatory bowel disease. *Inflamm Bowel Dis*. 2006;12(6):515–523.
48. Tanaka K, Sano K, Kobayashi M, Katsumura K, Ikeda T, Abe M. Demonstration of downregulation of α-smooth muscle actin in interferon-γ-treated myofibroblast by a novel cell-capture enzyme immunoassay. *Int Immunopharmacol*. 2001;1(4):769–775.
49. Sandbo N, Taurin S, Yau DM, Kregel S, Mitchell R, Dulin NO. Downregulation of smooth muscle alpha-actin expression by bacterial lipopolysaccharide. *Cardiovasc Res*. 2007;74(2):262–269.
50. Takeuchi K. Prophylactic effects of prostaglandin E on NSAID-induced enteropathy-role of EP4 receptors in its protective and healing-promoting effects. *Curr Opin Pharmacol*. 2014;19C:38–45.
51. Gately S, Li WW. Multiple roles of COX-2 in tumor angiogenesis: a target for antiangiogenic therapy. *Semin Oncol*. 2004;31(2 suppl 7):2–11.
52. Wang J, et al. VEGF expression is augmented by hypoxiainduced PGIS in human fibroblasts. *Int J Oncol*. 2013;43(3):746–754.
53. Park DW, et al. Activation of toll-like receptor 4 modulates vascular endothelial growth factor synthesis through prostacyclin-IP signaling. *Biochem Biophys Res Commun*. 2007;362(4):1090–1095.
54. Whittle BJ, Silverstein AM, Mottola DM, Clapp LH. Binding and activity of the prostacyclin receptor (IP) agonists, treprostinil and iloprost, at human prostanoid receptors: treprostinil is a potent DP1 and EP2 agonist. *Biochem Pharmacol*. 2012;84(1):68–75.
55. Kiriyama M, Ushikubi F, Kobayashi T, Hirata M, Sugimoto Y, Narumiya S. Ligand binding specificities of the eight types and subtypes of the mouse prostanoid receptors expressed in Chinese hamster ovary cells. *Br J Pharmacol*. 1997;122(2):217–224.
56. Abramovitz M, et al. The utilization of recombinant prostanoid receptors to determine the affinities and selectivities of prostaglandins and related analogs. *Biochim Biophys Acta*. 2000;1483(2):285–293.
57. Worthley DL, et al. Gremlin 1 identifies a skeletal stem cell with bone, cartilage, and reticular stromal potential. *Cell*. 2015;160(1–2):269–284.
58. Morham SG, et al. Prostaglandin synthase 2 gene disruption causes severe renal pathology in the mouse. *Cell*. 1995;83(3):473–482.